Electronic Supplementary Information

Tuning the Chemical Properties of Europium Complexes as Downshifting Agents for Copper Indium Gallium Selenide Solar Cells

Anatolie Gavriluta [a,b,c,], Thomas Fix [b,]*, Aline Nonat [c,]*, Abdelilah Slaoui [b], Jean-François Guillemoles [d,a], Loïc J. Charbonnière [c]*

[a] Institut Photovoltaïque d'Ile de France (IPVF), 8 rue de la Renaissance, 92160 Antony, France

[b] ICube Laboratory, Université de Strasbourg and CNRS, 23 rue du Loess BP 20 CR, 67037 Strasbourg Cedex 2, France

[c] LIMAA, IPHC, UMR 7178 CNRS, Université de Strasbourg, ECPM, 25 rue Becquerel, 67087 Strasbourg Cedex, France

[d] EDF R&D, IRDEP, Institute of R&D on Photovoltaic Energy, UMR 7174, CNRS-EDF-Chimie ParisTech, 6 Quai Watier-BP 49, 78401 Chatou Cedex, France

Summary

NMR spectroscopy

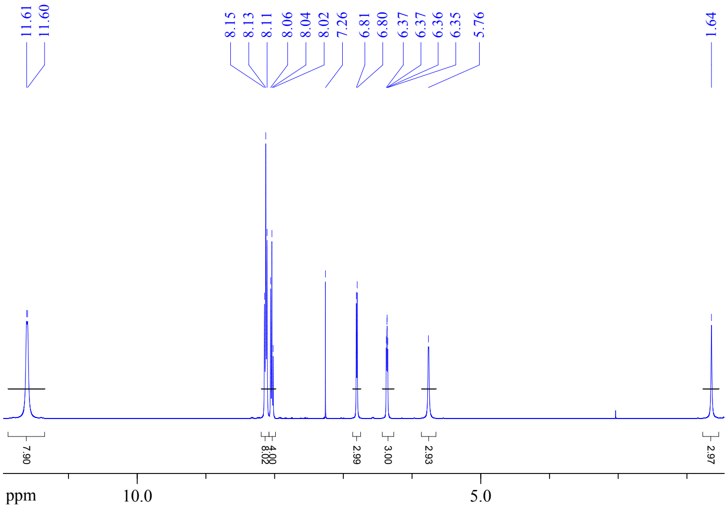

Figure S1. ^{1}H NMR spectrum of $[Eu(TTA)_3(DBSO)_2]$

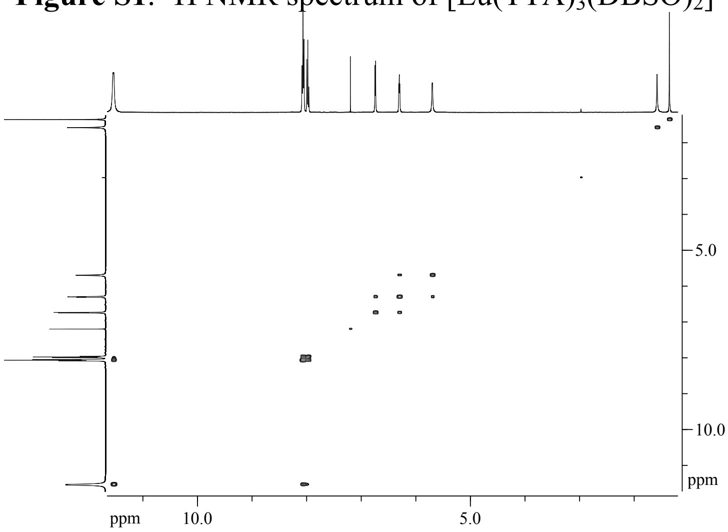

Figure S2. ^{1}H-^{1}H COSY NMR spectrum of $[Eu(TTA)_3(DBSO)_2]$

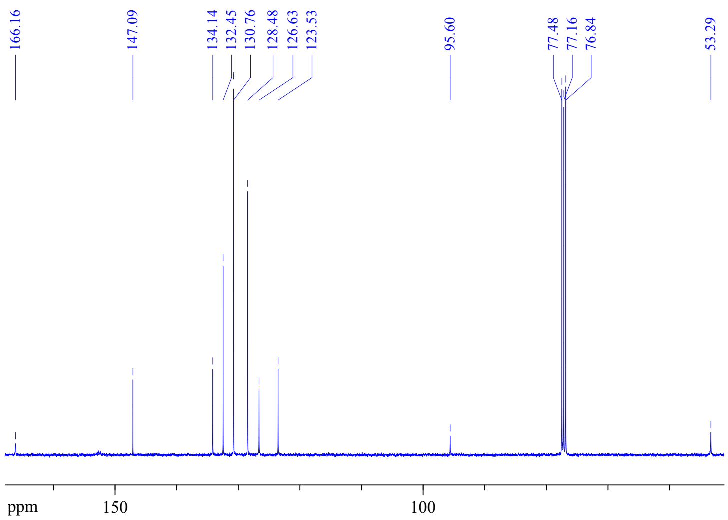

Figure S3. ^{13}C NMR spectrum of $[Eu(TTA)_3(DBSO)_2]$

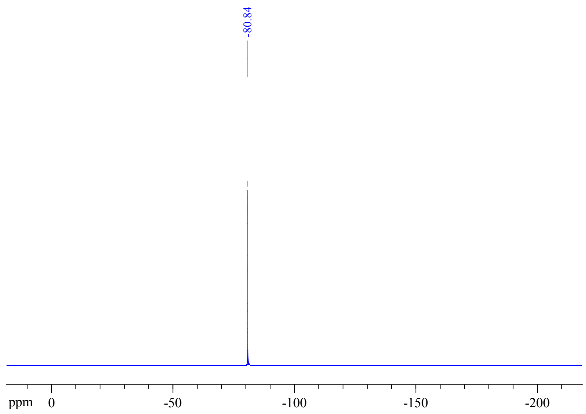

Figure S4. ^{19}F NMR spectrum of [Eu(TTA)$_3$(DBSO)$_2$]

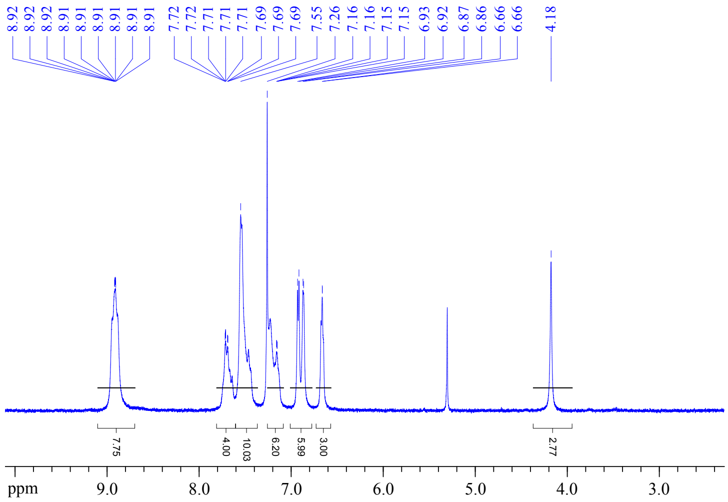

Figure S5. ^{1}H NMR spectrum of [Eu(TTA)$_3$(DPEPO)]

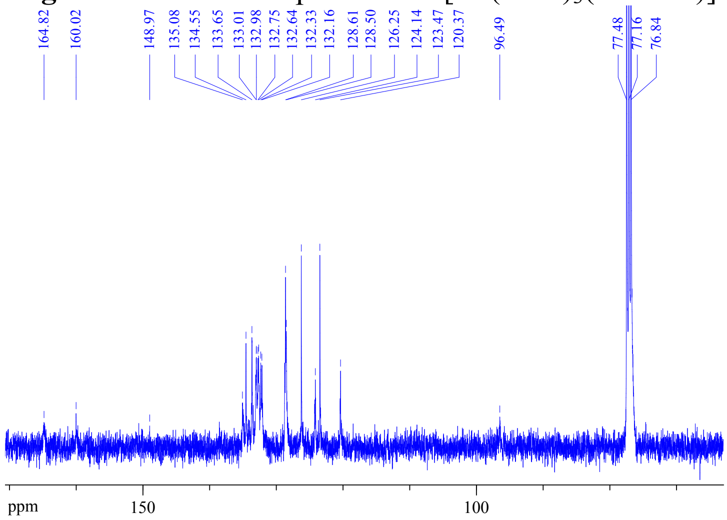

Figure S5. ^{13}C NMR spectrum of [Eu(TTA)$_3$(DPEPO)]

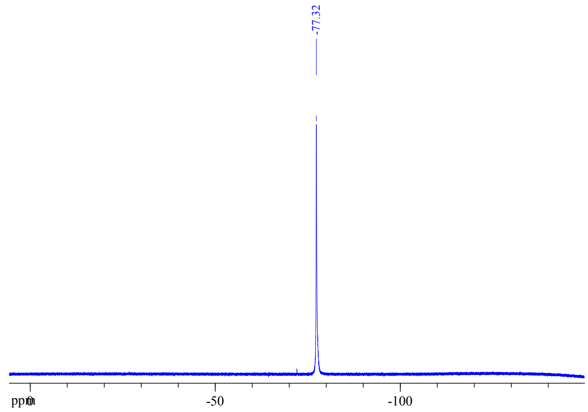

Figure S6. ^{19}F NMR spectrum of [Eu(TTA)$_3$(DPEPO)]

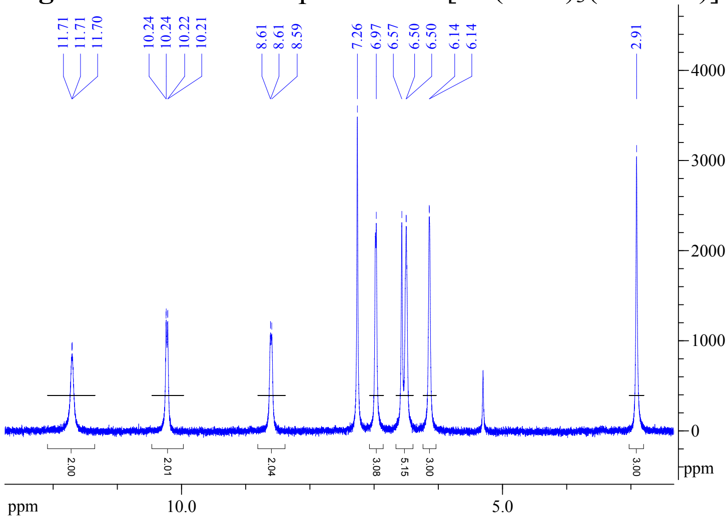

Figure S7. ^{1}H NMR spectrum of [Eu(TTA)$_3$(EPhen)]

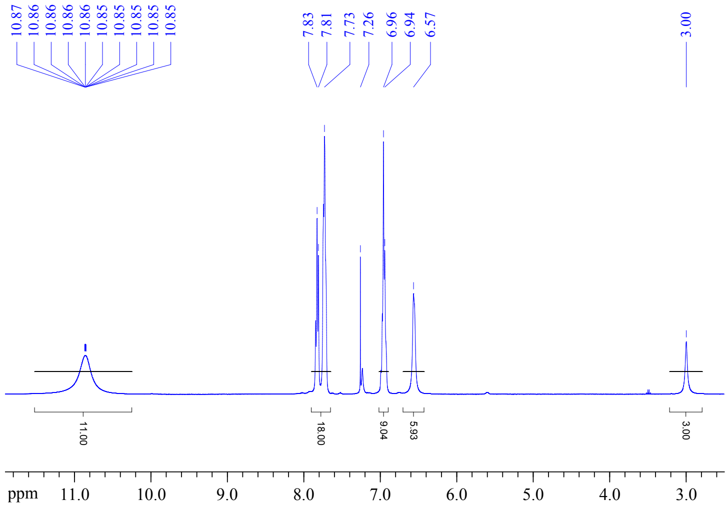

Figure S8. ^{1}H NMR spectrum of [Eu(PTA)$_3$(TPPO)$_2$]

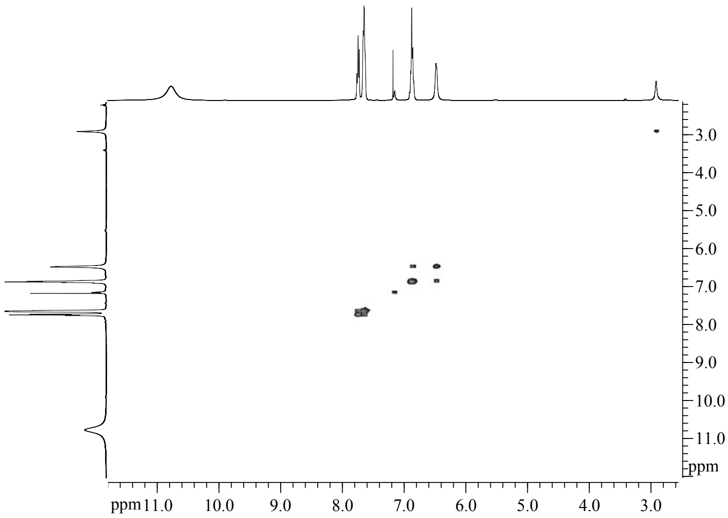

Figure S9. ^{1}H-^{1}H COSY NMR spectrum of $[Eu(PTA)_3(TPPO)_2]$

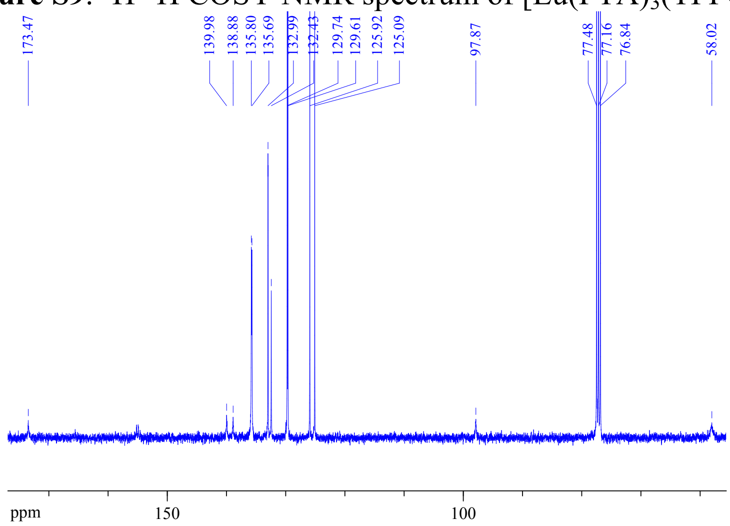

Figure S10. ^{13}C NMR spectrum of $[Eu(PTA)_3(TPPO)_2]$

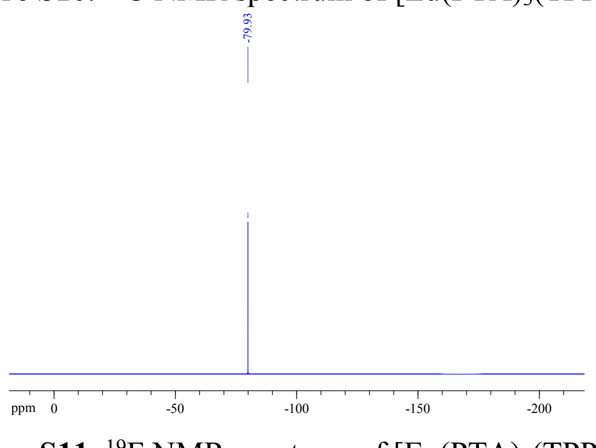

Figure S11. ^{19}F NMR spectrum of $[Eu(PTA)_3(TPPO)_2]$

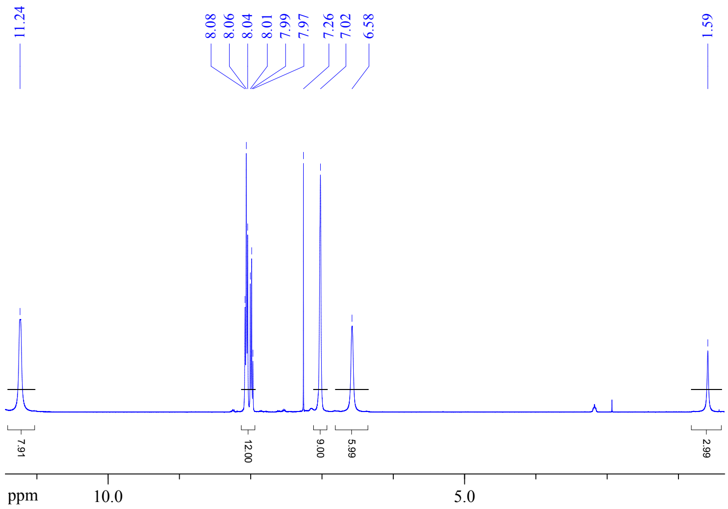

Figure S12. [1]H NMR spectrum of [Eu(PTA)$_3$(DBSO)$_2$]

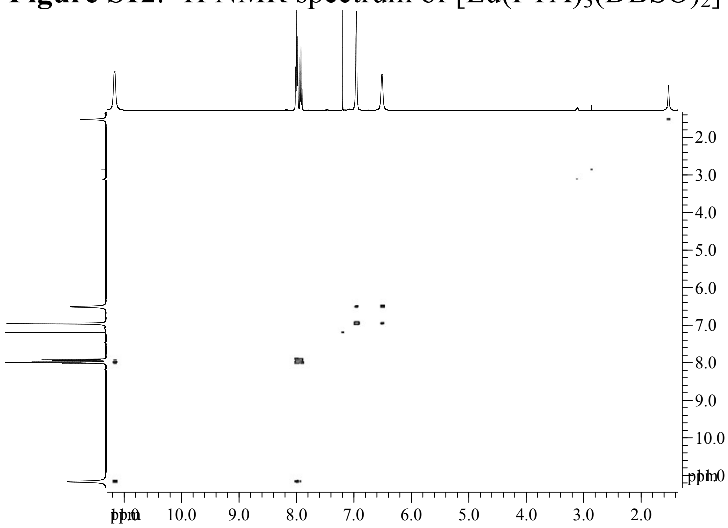

Figure S13. [1]H-[1]H COSY NMR spectrum of [Eu(PTA)$_3$(DBSO)$_2$]

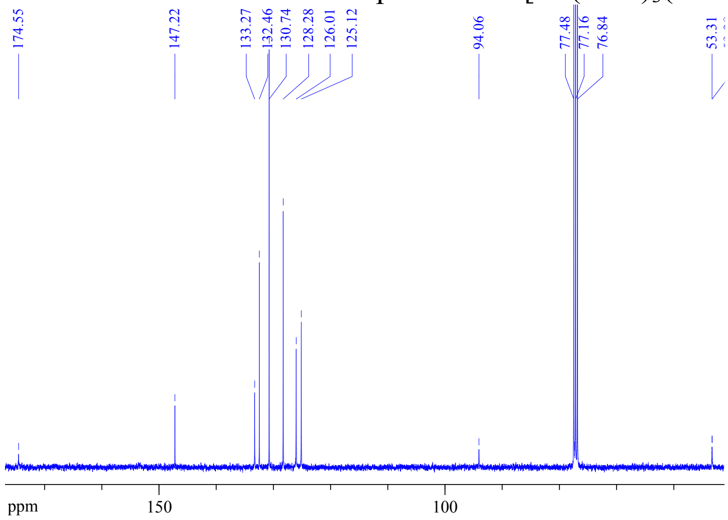

Figure S14. [13]C NMR spectrum of [Eu(PTA)$_3$(DBSO)$_2$]

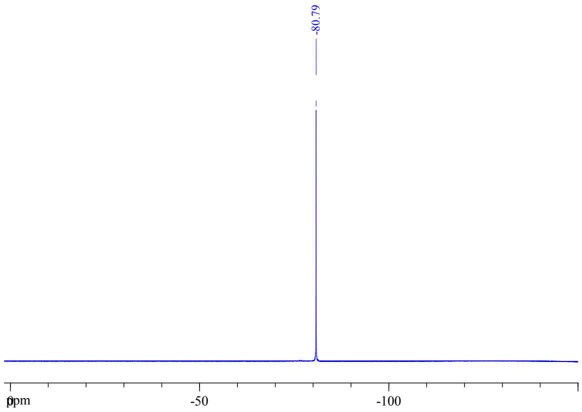

Figure S15. ^{19}F NMR spectrum of $[Eu(PTA)_3(DBSO)_2]$

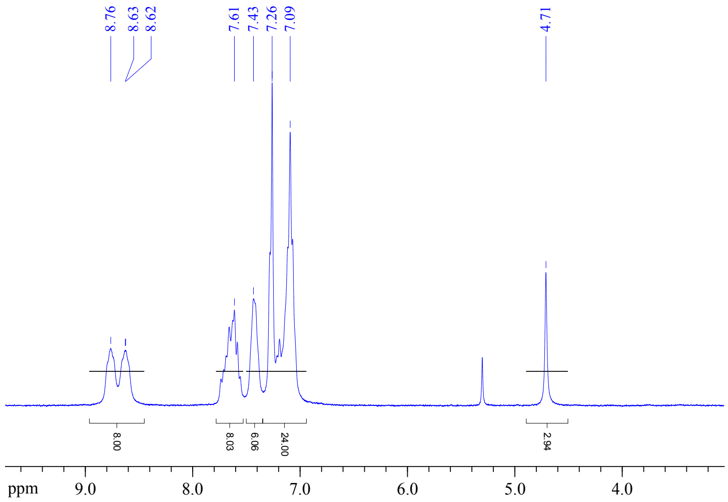

Figure S16. ^{1}H NMR spectrum of $[Eu(PTA)_3(DPEPO)]$

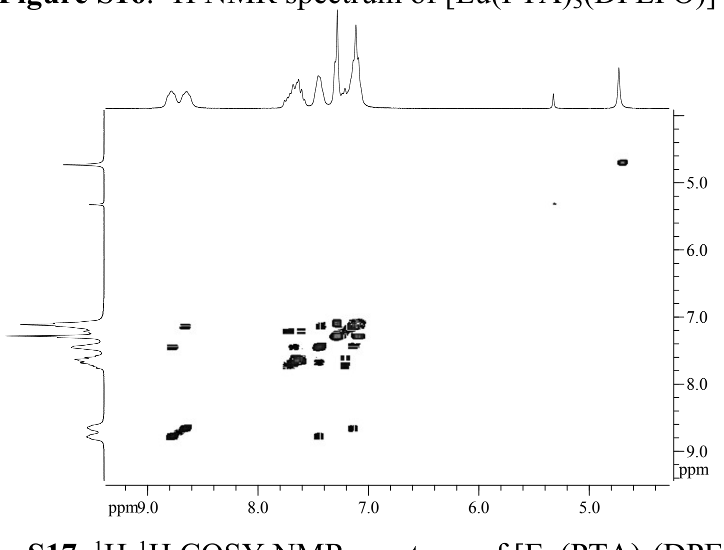

Figure S17. ^{1}H-^{1}H COSY NMR spectrum of $[Eu(PTA)_3(DPEPO)]$

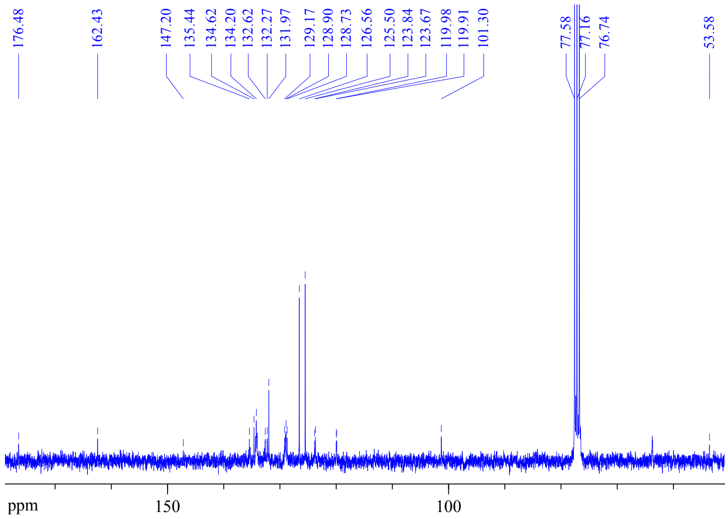

Figure S18. ^{13}C NMR spectrum of $[Eu(PTA)_3(DPEPO)]$

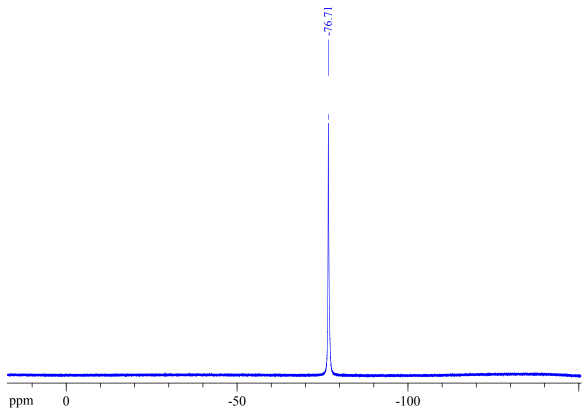

Figure S19. ^{19}F NMR spectrum of $[Eu(PTA)_3(DPEPO)]$

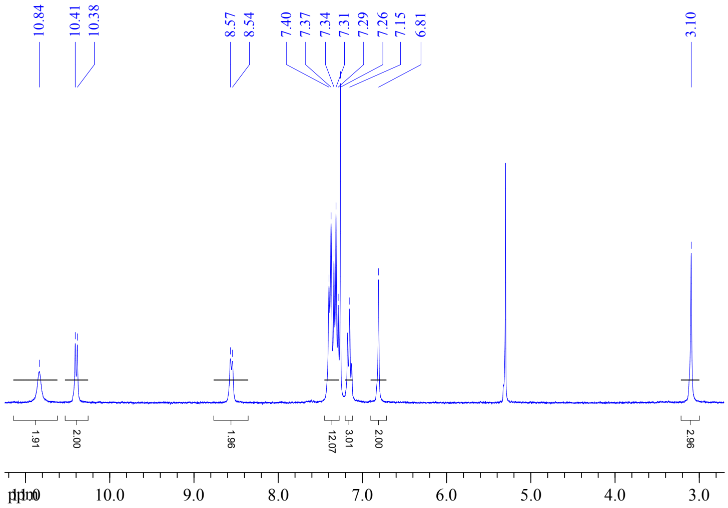

Figure S20. ^{1}H NMR spectrum of $[Eu(PTA)_3(EPhen)]$

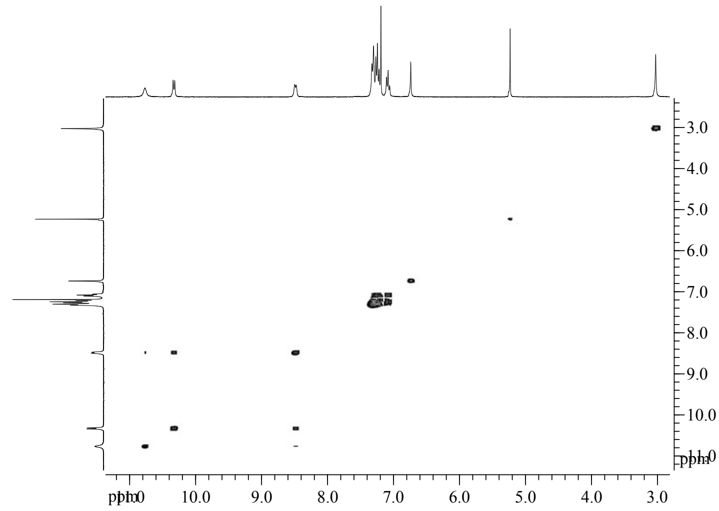

Figure S21. ¹H-¹H COSY NMR spectrum of [Eu(PTA)$_3$(EPhen)]

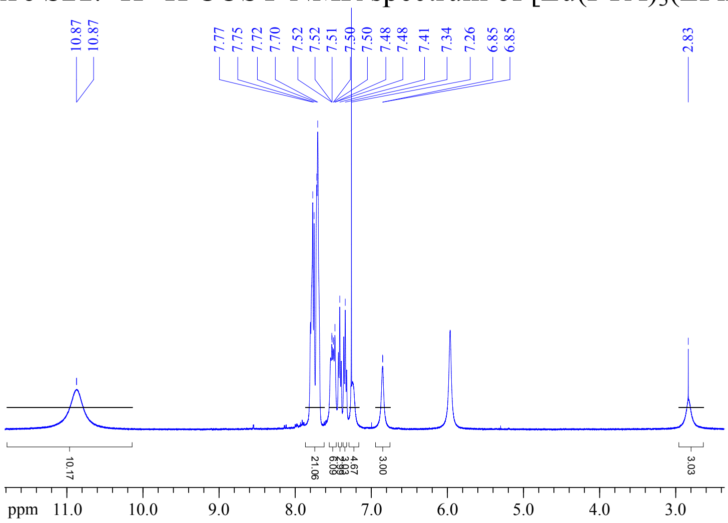

Figure S22. ¹H NMR spectrum of [Eu(NTA)$_3$(TPPO)$_2$]

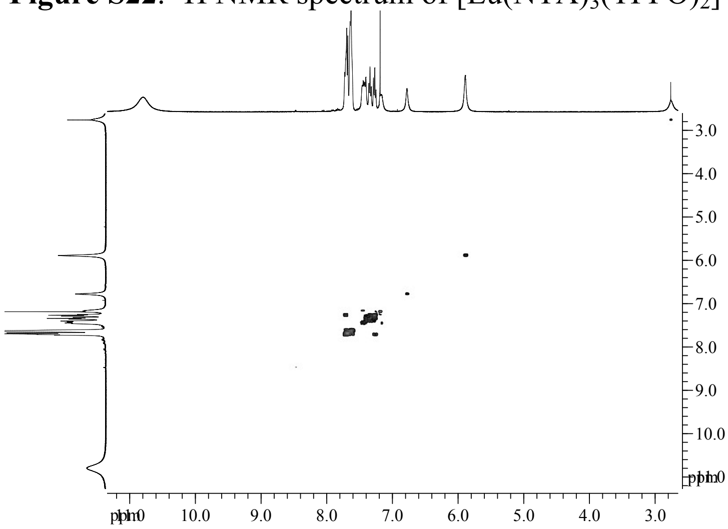

Figure S23. ¹H-¹H COSY NMR spectrum of [Eu(NTA)$_3$(TPPO)$_2$]

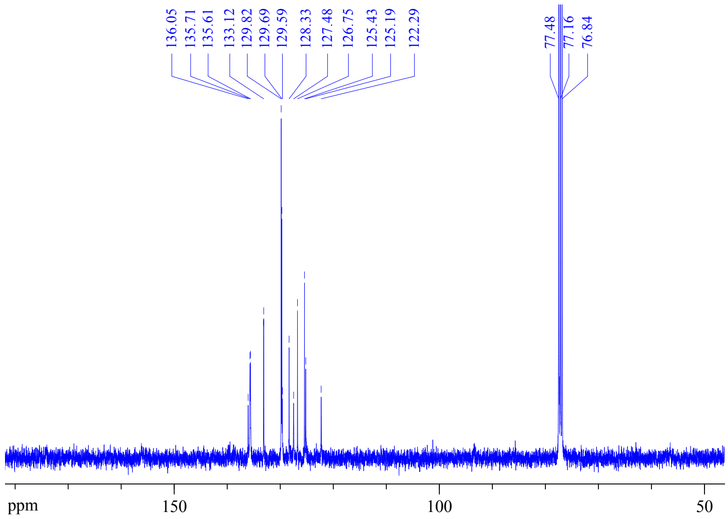

Figure S24. ^{13}C NMR spectrum of $[Eu(NTA)_3(TPPO)_2]$

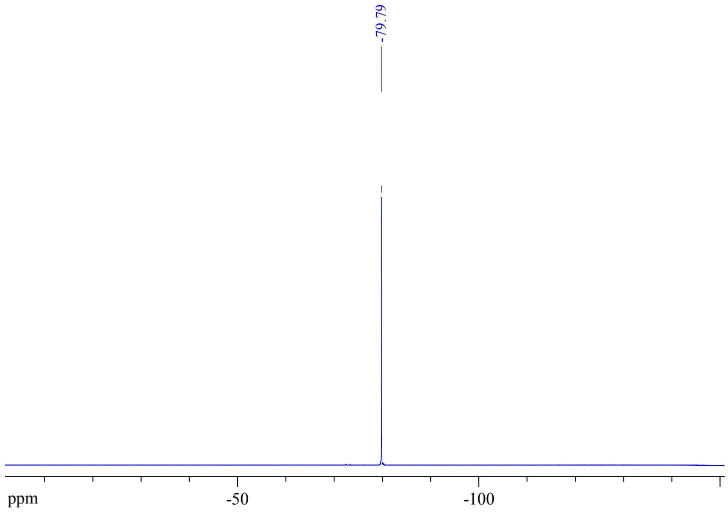

Figure S25. ^{19}F NMR spectrum of $[Eu(NTA)_3(TPPO)_2]$

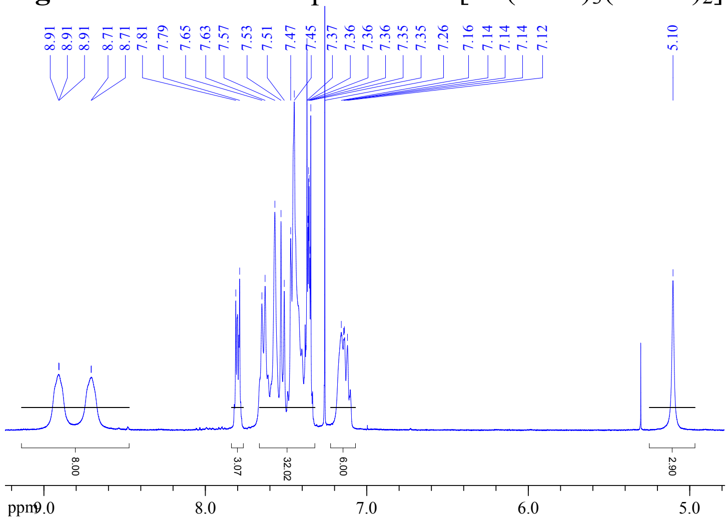

Figure S26. ^{1}H NMR spectrum of $[Eu(NTA)_3(DPEPO)]$

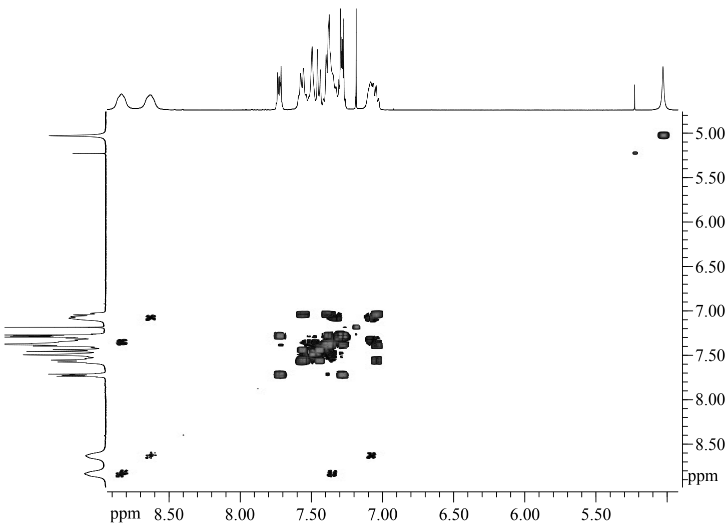

Figure S27. ^{1}H-^{1}H COSY NMR spectrum of $[Eu(NTA)_3(TPPO)_2]$

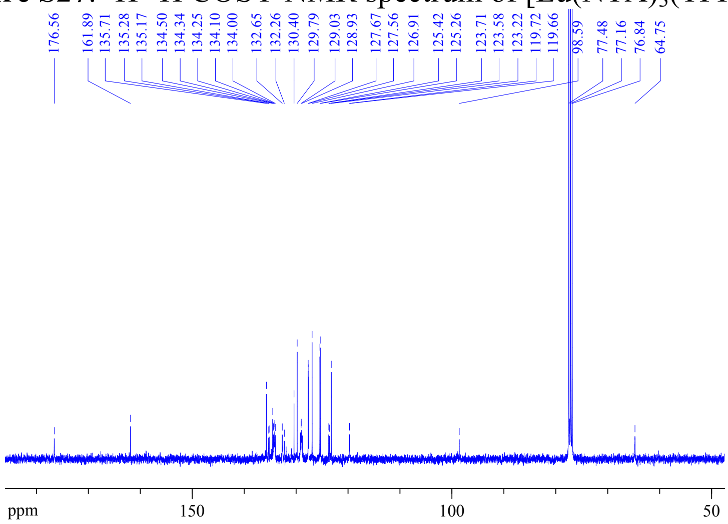

Figure S28. ^{13}C NMR spectrum of $[Eu(NTA)_3(TPPO)_2]$

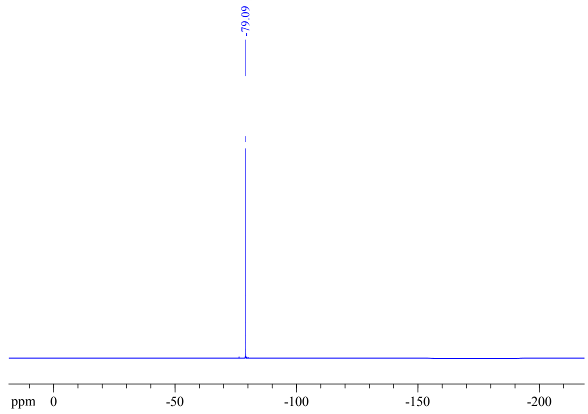

Figure S29. ^{19}F NMR spectrum of $[Eu(NTA)_3(TPPO)_2]$

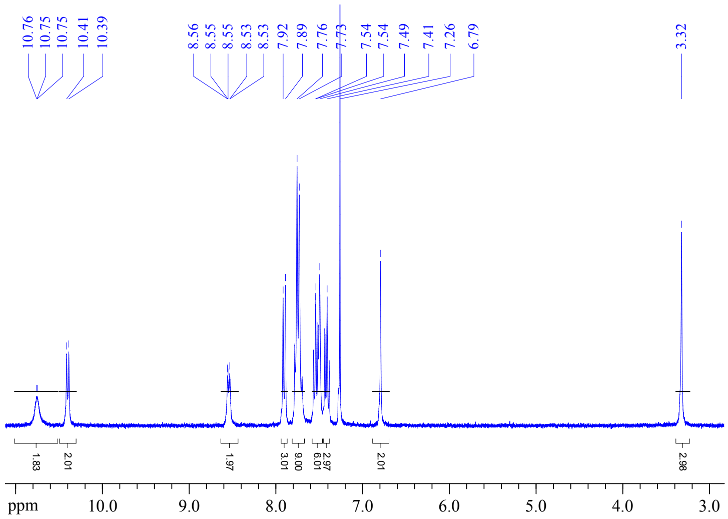

Figure S30. ^{1}H NMR spectrum of [Eu(NTA)$_3$(EPhen)]

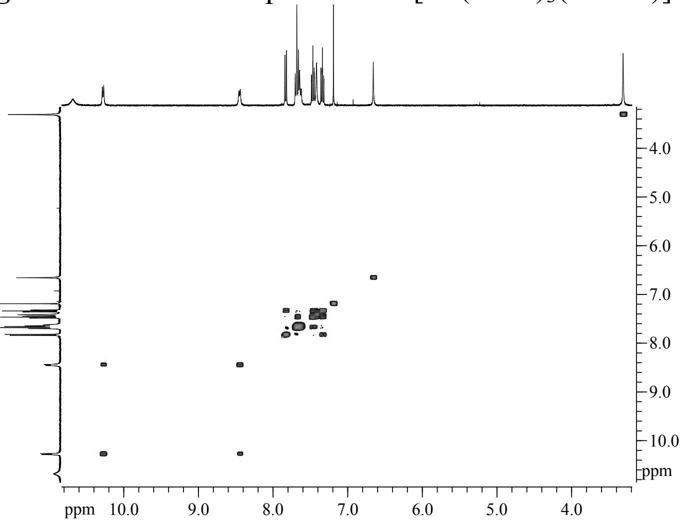

Figure S31. ^{1}H-^{1}H COSY NMR spectrum of [Eu(NTA)$_3$(EPhen)]

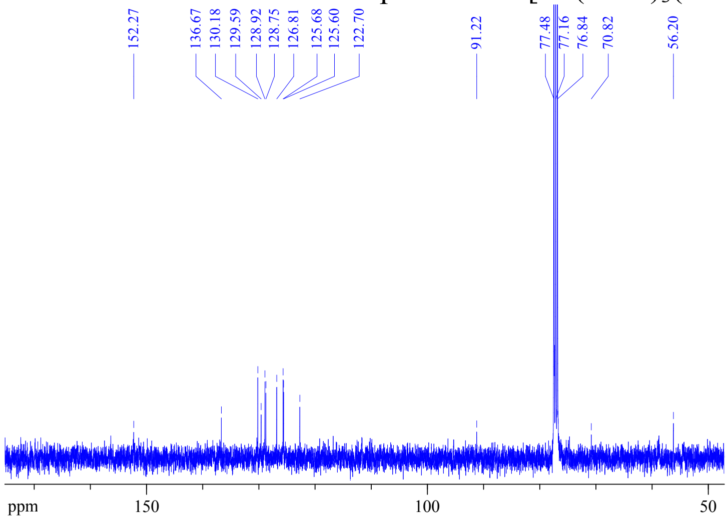

Figure S32. ^{13}C NMR spectrum of [Eu(NTA)$_3$(EPhen)]

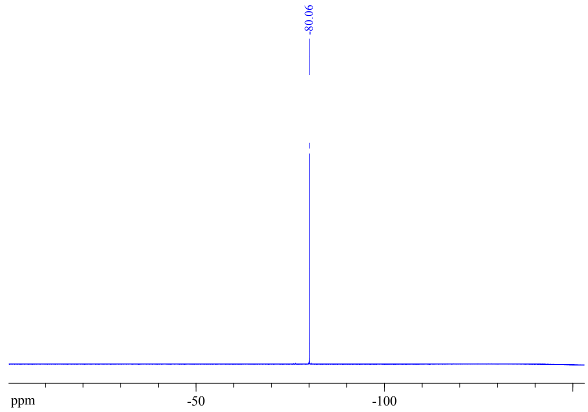

Figure S33. ^{19}F NMR spectrum of [Eu(NTA)$_3$(EPhen)]

Infrared spectroscopy

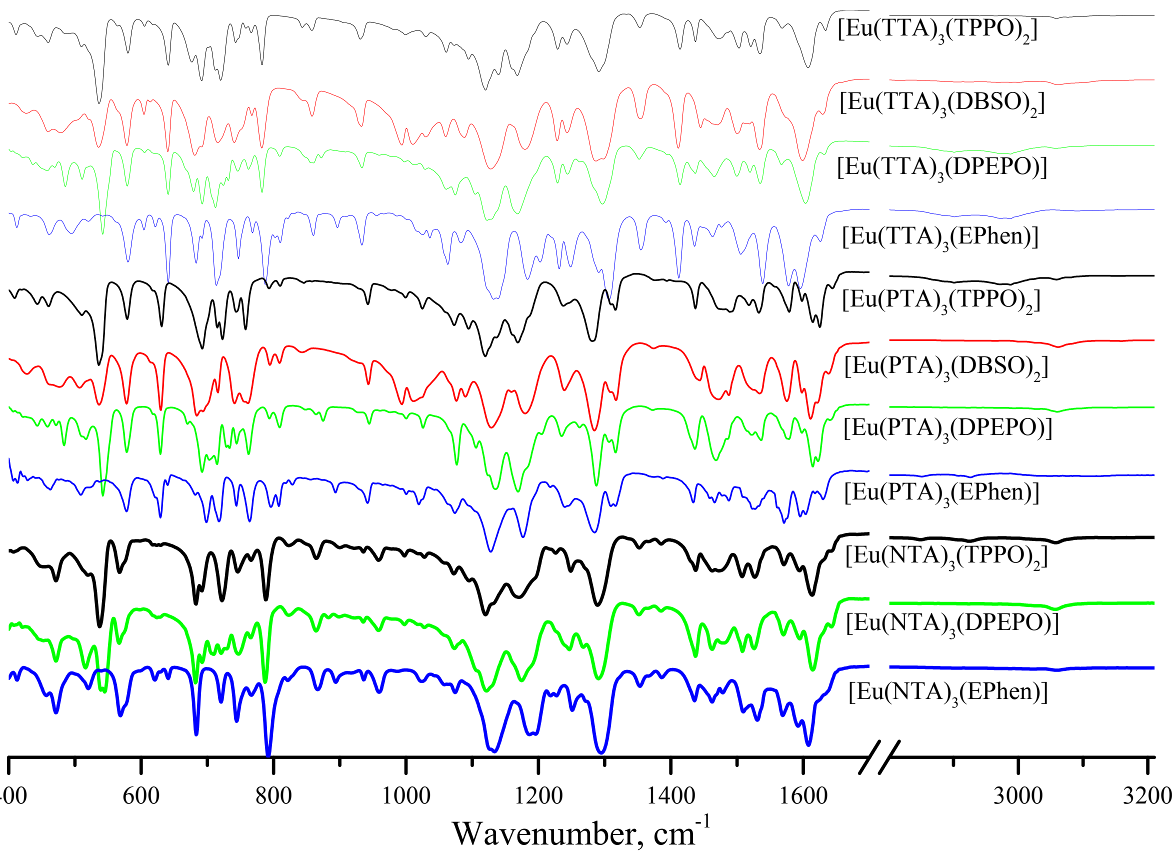

Figure S34. IR spectra of europium (III) coordination complexes studied in this work.

Photo-physical properties

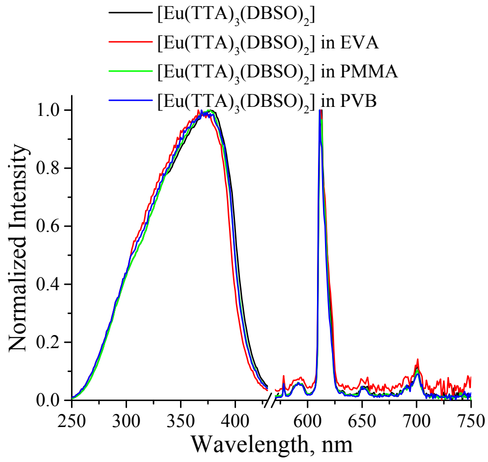

Figure S35. Excitation and emission spectra of $[Eu(TTA)_3(DBSO)_2]$ in solid state and encapsulated in EVA, PMMA and PVB. The excitation spectra were recorded by monitoring the $^5D_0 \rightarrow ^7F_2$ transition (λ_{em} = 613 nm), and for the emission spectra the λ_{ex} = 340 nm.

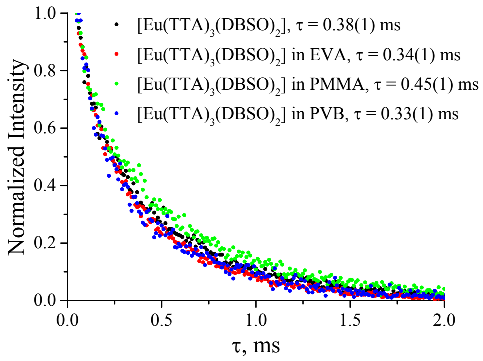

Figure S36. Photoluminescence decay (λ_{em} = 613 nm, λ_{ex} = 340 nm) of $[Eu(TTA)_3(DBSO)_2]$ in solid state and in different polymeric matrices.

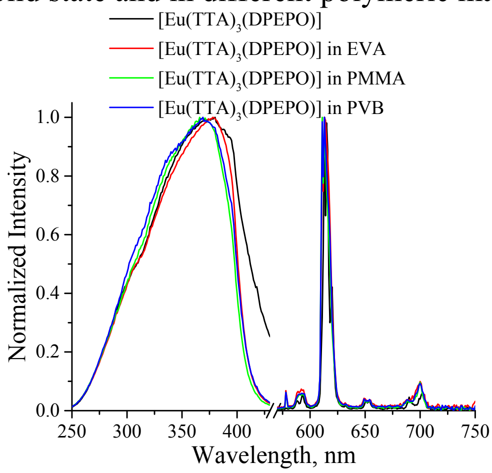

Figure S37. Excitation and emission spectra of $[Eu(TTA)_3(DPEPO)]$ in solid state and encapsulated in EVA, PMMA and PVB. The excitation spectra were recorded by monitoring the $^5D_0 \rightarrow ^7F_2$ transition (λ_{em} = 613 nm), and for the emission spectra the λ_{ex} = 340 nm.

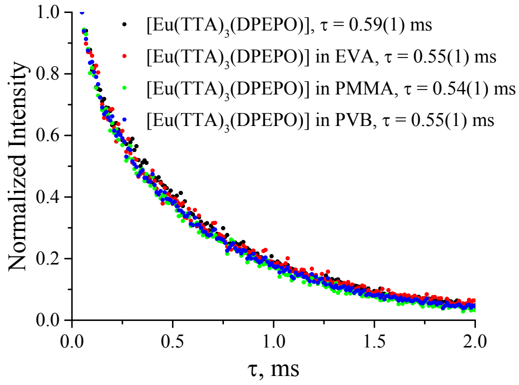

Figure S38. Photoluminescence decay (λ_{em} = 613 nm, λ_{ex} = 340 nm) of [Eu(TTA)$_3$(DPEPO)] in solid state and in different polymeric matrices.

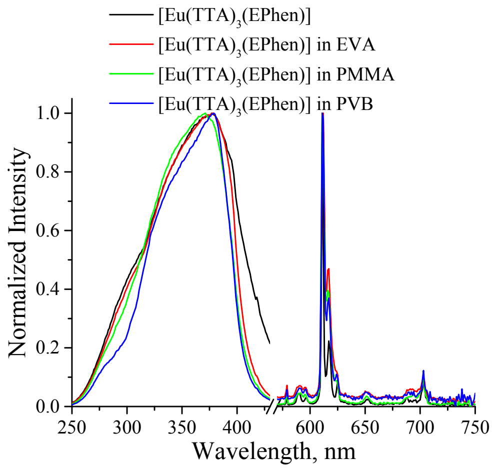

Figure S39. Excitation and emission spectra of [Eu(TTA)$_3$(EPhen)] in solid state and encapsulated in EVA, PMMA and PVB. The excitation spectra were recorded by monitoring the $^5D_0 \rightarrow ^7F_2$ transition (λ_{em} = 613 nm), and for the emission spectra the λ_{ex} = 340 nm.

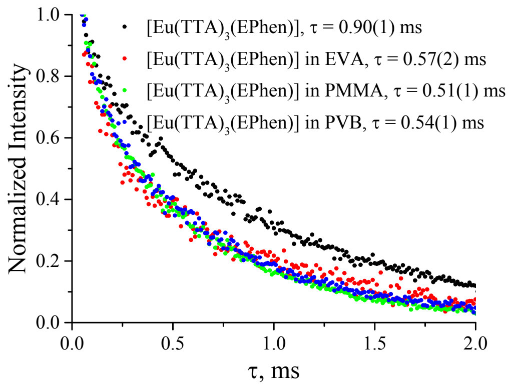

Figure S40. Photoluminescence decay (λ_{em} = 613 nm, λ_{ex} = 340 nm) of [Eu(TTA)$_3$(EPhen)] in solid state and in different polymeric matrices.

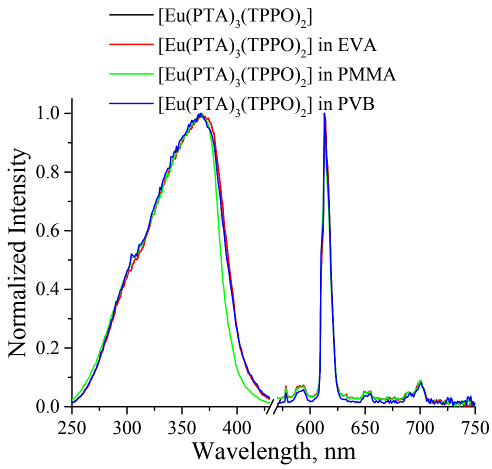

Figure S41. Excitation and emission spectra of [Eu(PTA)$_3$(TPPO)$_2$] in solid state and encapsulated in EVA, PMMA and PVB. The excitation spectra were recorded by monitoring the $^5D_0 \rightarrow ^7F_2$ transition (λ_{em} = 613 nm), and for the emission spectra the λ_{ex} = 340 nm.

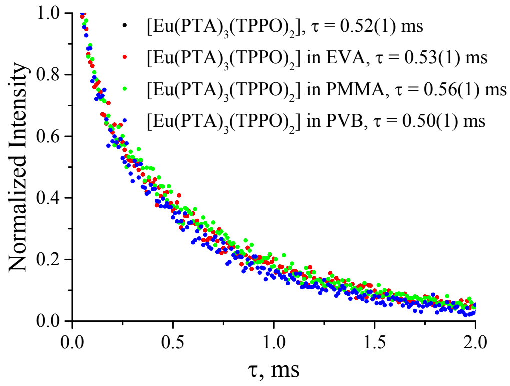

Figure S42. Photoluminescence decay (λ_{em} = 613 nm, λ_{ex} = 340 nm) of [Eu(PTA)$_3$(TPPO)$_2$] in solid state and in different polymeric matrices.

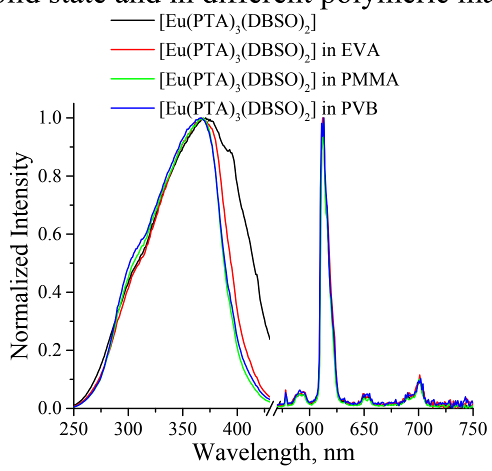

Figure S43. Excitation and emission spectra of [Eu(PTA)$_3$(DBSO)$_2$] in solid state and encapsulated in EVA, PMMA and PVB. The excitation spectra were recorded by monitoring the $^5D_0 \rightarrow ^7F_2$ transition (λ_{em} = 613 nm), and for the emission spectra the λ_{ex} = 340 nm.

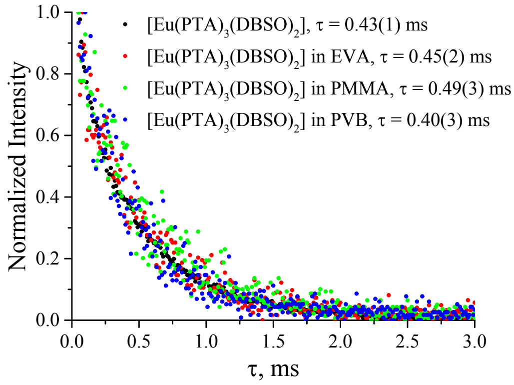

Figure S44. Photoluminescence decay (λ_{em} = 613 nm, λ_{ex} = 350 nm) of [Eu(PTA)$_3$(DBSO)$_2$] in solid state and in different polymeric matrices.

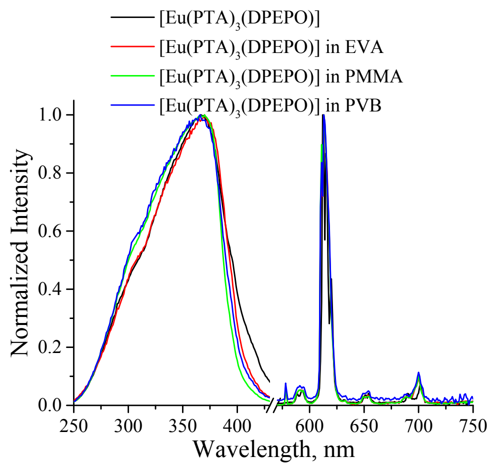

Figure S45. Excitation and emission spectra of [Eu(PTA)$_3$(DPEPO)] in solid state and encapsulated in EVA, PMMA and PVB. The excitation spectra were recorded by monitoring the $^5D_0 \rightarrow ^7F_2$ transition (λ_{em} = 613 nm), and for the emission spectra the λ_{ex} = 340 nm.

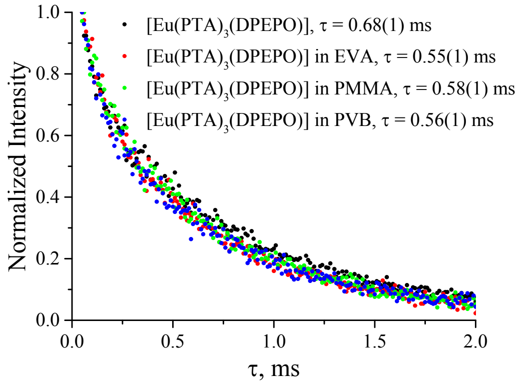

Figure S46. Photoluminescence decay (λ_{em} = 613 nm, λ_{ex} = 340 nm) of [Eu(PTA)$_3$(DPEPO)] in solid state and in different polymeric matrices.

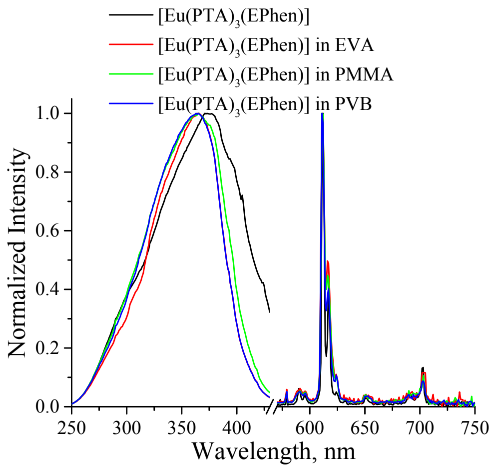

Figure S47. Excitation and emission spectra of [Eu(PTA)$_3$(EPhen)] in solid state and encapsulated in EVA, PMMA and PVB. The excitation spectra were recorded by monitoring the $^5D_0 \rightarrow {}^7F_2$ transition (λ_{em} = 613 nm), and for the emission spectra the λ_{ex} = 340 nm.

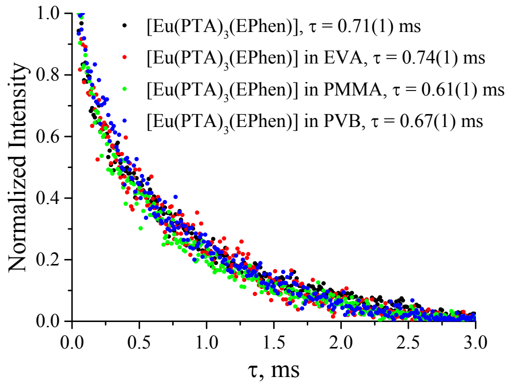

Figure S48. Photoluminescence decay (λ_{em} = 613 nm, λ_{ex} = 340 nm) of [Eu(PTA)$_3$(EPhen)] in solid state and in different polymeric matrices.

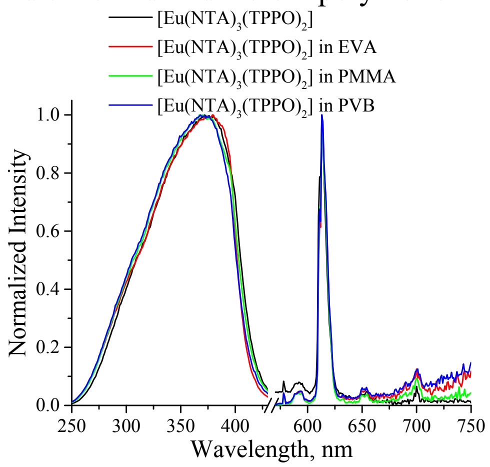

Figure S49. Excitation and emission spectra of [Eu(NTA)$_3$(TPPO)$_2$] in solid state and encapsulated in EVA, PMMA and PVB. The excitation spectra were recorded by monitoring the $^5D_0 \rightarrow {}^7F_2$ transition (λ_{em} = 613 nm), and for the emission spectra the λ_{ex} = 340 nm.

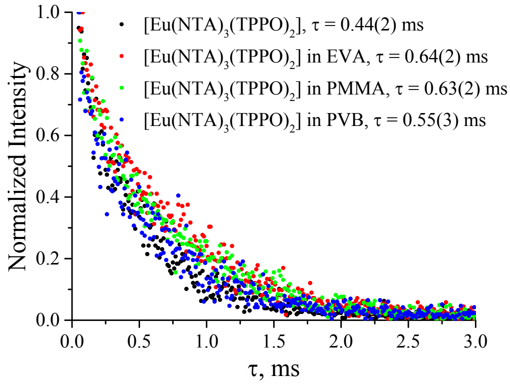

Figure S50. Photoluminescence decay (λ_{em} = 613 nm, λ_{ex} = 340 nm) of [Eu(NTA)$_3$(TPPO)$_2$] in solid state and in different polymeric matrices.

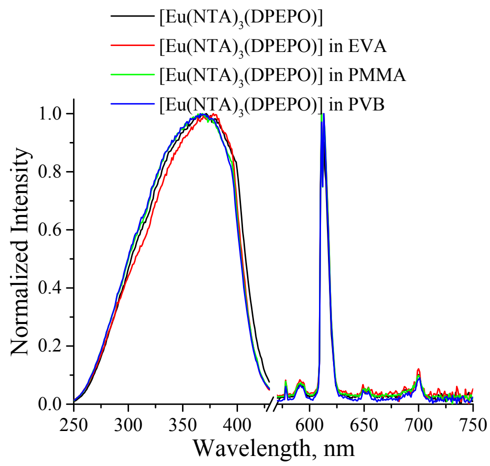

Figure S51. Excitation and emission spectra of [Eu(NTA)$_3$(DPEPO)] in solid state and encapsulated in EVA, PMMA and PVB. The excitation spectra were recorded by monitoring the $^5D_0 \rightarrow {}^7F_2$ transition (λ_{em} = 613 nm), and for the emission spectra the λ_{ex} = 340 nm.

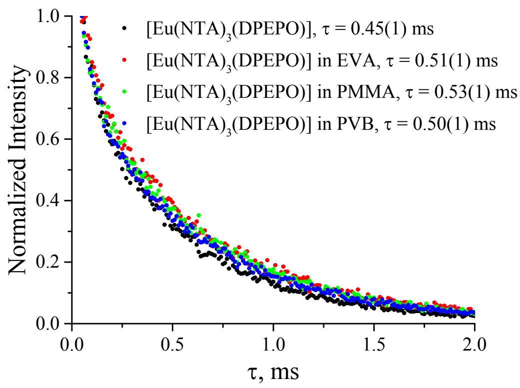

Figure S52. Photoluminescence decay (λ_{em} = 613 nm, λ_{ex} = 340 nm) of [Eu(NTA)$_3$(DPEPO)] in solid state and in different polymeric matrices.

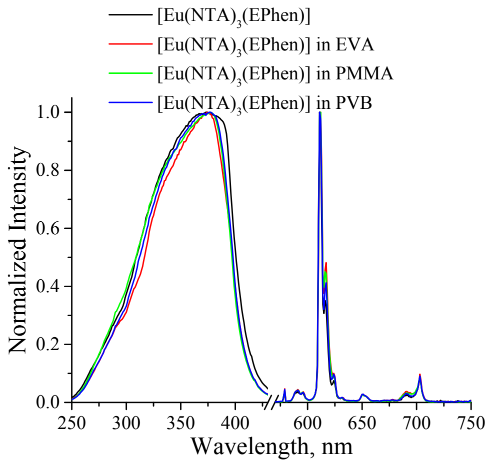

Figure S53. Excitation and emission spectra of [Eu(NTA)$_3$(EPhen)] in solid state and encapsulated in EVA, PMMA and PVB. The excitation spectra were recorded by monitoring the $^5D_0 \rightarrow ^7F_2$ transition (λ_{em} = 613 nm), and for the emission spectra the λ_{ex} = 340 nm.

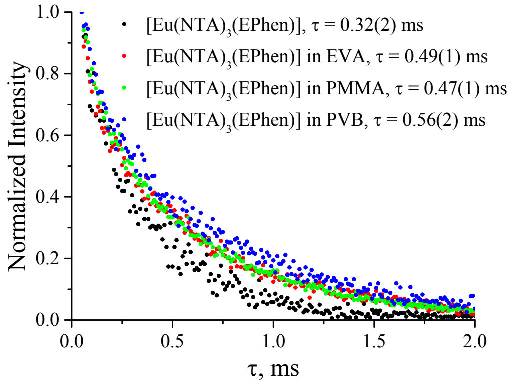

Figure S54. Photoluminescence decay (λ_{em} = 613 nm, λ_{ex} = 340 nm) of [Eu(NTA)$_3$(EPhen)] in solid state and in different polymeric matrices.

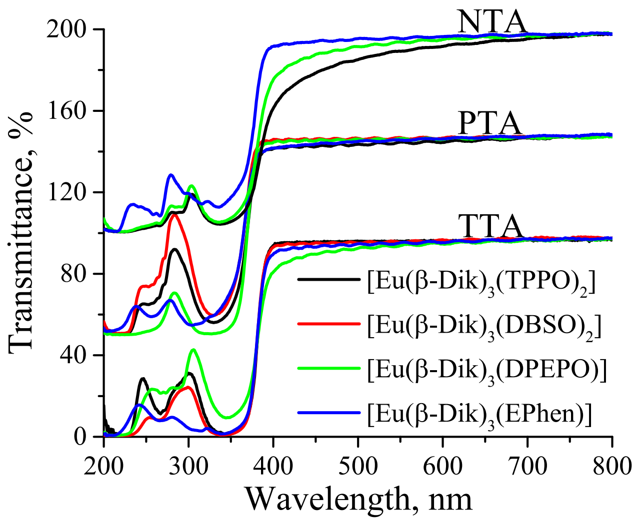

Figure S55. Transmittance spectra of europium (III) complexes embedded into EVA.

Spectral response

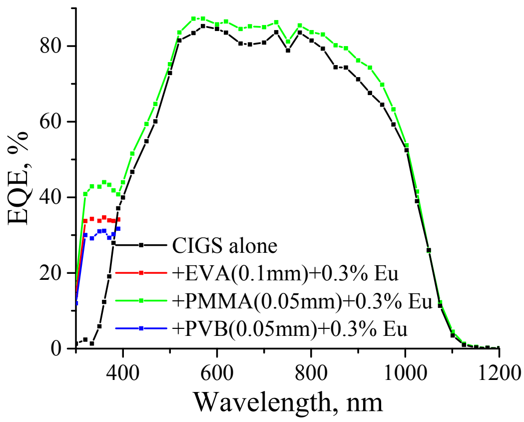

Figure S56. EQE spectra of CIGS solar cells encapsulated by different polymers doped with [Eu(TTA)$_3$(DBSO)$_2$].

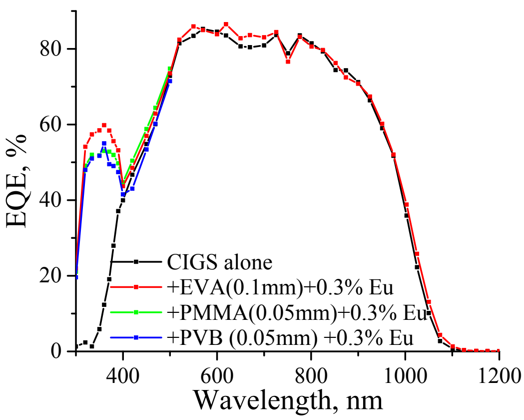

Figure S57. EQE spectra of CIGS solar cells encapsulated by different polymers doped with [Eu(TTA)$_3$(DPEPO)].

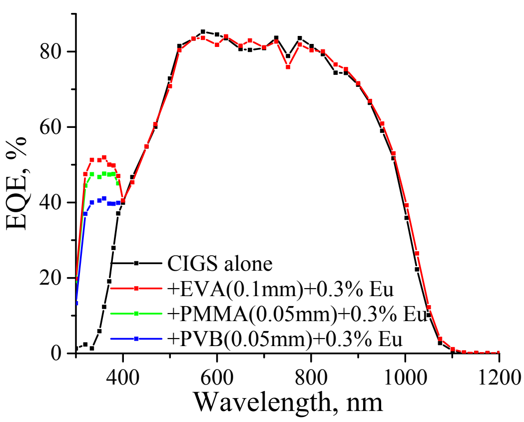

Figure S58. EQE spectra of CIGS solar cells encapsulated by different polymers doped with [Eu(TTA)$_3$(EPhen)].

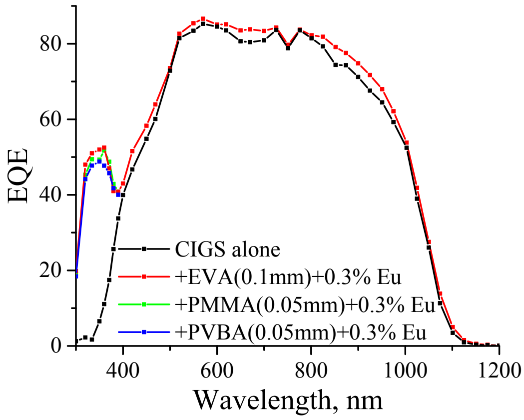

Figure S59. EQE spectra of CIGS solar cells encapsulated by different polymers doped with [Eu(PTA)$_3$(TPPO)$_2$].

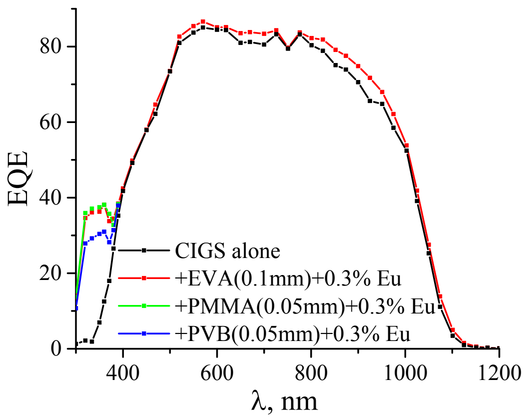

Figure S60. EQE spectra of CIGS solar cells encapsulated by different polymers doped with [Eu(PTA)$_3$(DBSO)$_2$].

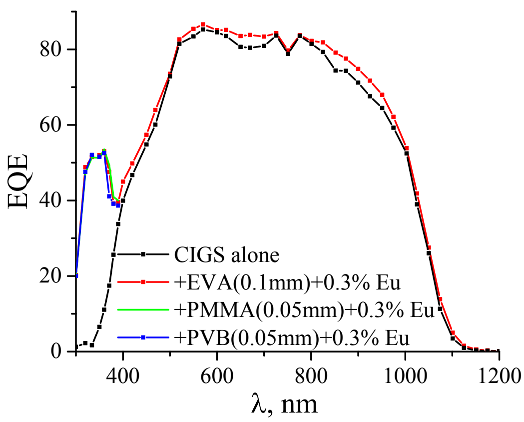

Figure S61. EQE spectra of CIGS solar cells encapsulated by different polymers doped with [Eu(PTA)$_3$(DPEPO)].

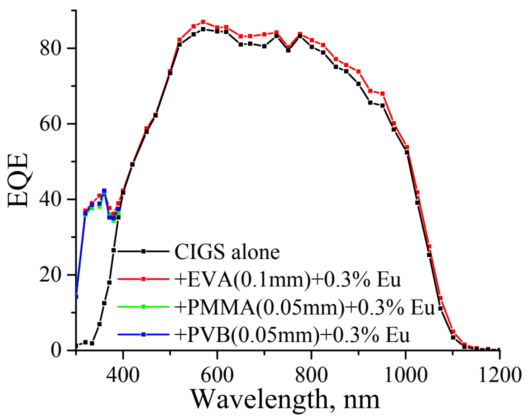

Figure S62. EQE spectra of CIGS solar cells encapsulated by different polymers doped with [Eu(PTA)$_3$(EPhen)].

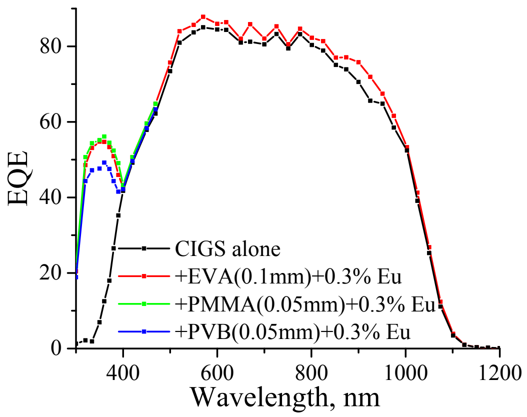

Figure S63. EQE spectra of CIGS solar cells encapsulated by different polymers doped with [Eu(NTA)$_3$(TPPO)$_2$].

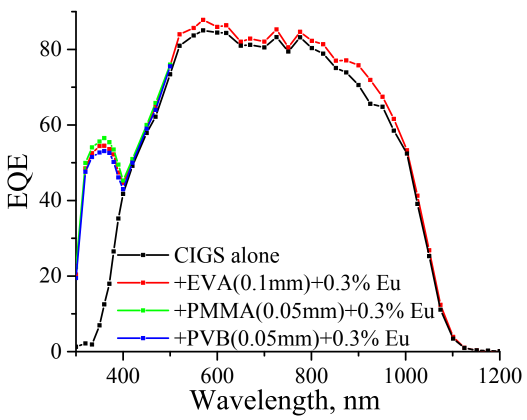

Figure S64. EQE spectra of CIGS solar cells encapsulated by different polymers doped with [Eu(NTA)$_3$(DPEPO)].

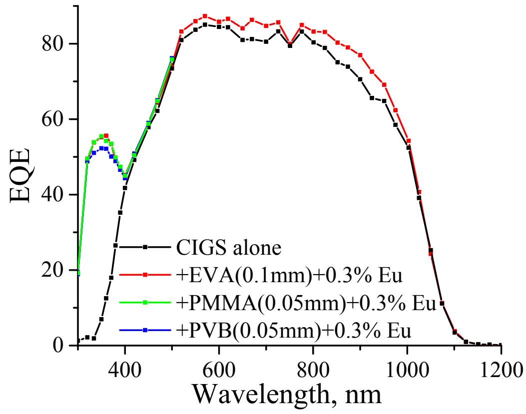

Figure S65. EQE spectra of CIGS solar cells encapsulated by different polymers doped with [Eu(NTA)$_3$(EPhen)].